Engineering Contactless Particle–Particle Interactions in Active Microswimmers

*Amir Nourhani, Daniel Brown, Nicholas Pletzer, and John G. Gibbs**

Artificial self-propelled colloidal particles have recently served as effective building blocks for investigating many dynamic behaviors exhibited by nonequilibrium systems. However, most studies have relied upon excluded volume interactions between the active particles. Experimental systems in which the mobile entities interact over long distances in a well-defined and controllable manner are valuable so that new modes of multiparticle dynamics can be studied systematically in the laboratory. Here, a system of self-propelled microscale Janus particles is engineered to have contactless particle–particle interactions that lead to long-range attraction, short-range repulsion, and mutual alignment between adjacent swimmers. The unique modes of motion that arise can be tuned by modulating the system's parameters.

Active propulsion and the powering of nanomotors,[1–8] microbots,[3,9–14] and nanomachines[15,16] have been the subject of intense research over the past decade. These studies have not only led to better understanding of nonequilibrium active matter,[17] but have also facilitated numerous practical applications[18,19] such as small scale cargo delivery,[20–24] sensing,[25–27] and nanoscale actuation within complex fluids.[28] Currently, the behavior of individual active particles is well documented and mostly understood. However, as this field advances, greater emphasis is being placed upon investigating and engineering the interactions between swimmers,[4,29–33] for the next wave of advanced applications. The majority of the available studies on the interactions between active colloids have demonstrated self-assembly via direct contact excluded volume interactions and through powered motility of the mobile entities,[34–37] e.g., the particles come into contact to form self-assembled clusters that translate and rotate. Here, we demonstrate a novel paradigm for designing contactless interparticle interactions in artificial microscale systems. We primarily focus upon pair-interactions in which competing forces lead to long-range attraction and short-range repulsion between the particles resulting from active propulsion combined with alignment, and magnetic dipole–dipole interactions, respectively. However, we also demonstrate modes of motion unique to this system including contactless cargo delivery and "chasing" behavior as well as loosely bound multiparticle clusters in which the individual swimmers are free to rearrange themselves within the group due to the contactless nature of the interparticle interactions.

Our system requires the particles to undergo self-propulsion while at the same time aligning with an external magnetic field. In order to produce such structures, we deposited both magnetic nickel (Ni) and catalytic platinum (Pt) by physical vapor deposition onto silica microspheres of diameter 2.2 μm, thus forming "Janus" spheres,[38,39] as shown in **Figure 1**. In this communication, we define the exposed silica side of the Janus sphere as the "head." On the other half, the two metallic layers approximately form prolate spheroidal half-shells that cap one side of the dielectric spheres (see Supporting Information). Since we deposited the two metals sequentially using electron-beam evaporation, in which the material deposits onto the spheres in a ballistic manner, we expect the similarity between the particles to be sufficient to avoid significant differences in the catalytic and magnetic properties.

In a solution of hydrogen peroxide, Janus spheres with a Pt half-shell undergo self-propulsion,[40,41] and therefore, we deposited the Pt on top of the Ni so that it would be on the outer surface, as shown in Figure 1, and thus the catalyst is exposed to the chemical. The Janus spheres were removed from the surface after deposition, were left unmagnetized, and were allowed to settle to the planar surface of an Si(100) wafer in water and hydrogen peroxide. We did not magnetize the particles before dispersal as magnetized Janus spheres were observed to rapidly self-assembled as a result of their permanent dipoles from the ferromagnetic Ni. As a demonstration, video V1 in the Supporting Information shows the result of removing a magnetic field and the subsequent self-assembly of several magnetized particles.

In the presence of hydrogen peroxide and in the absence of an external magnetic field, the unmagnetized particles moved confined by gravity close to the horizontal surface toward the "Janus director," i.e., the vector pointing from the metallic to the dielectric hemisphere, and perpendicular to the plane bisecting the two hemispheres, as shown on the right side of Figure 1. We note this alignment of the Janus director in the absence of a magnetic field is due to interactions between the particles and the solid boundary.[42,43] In our system, isolated particles self-propelled in hydrogen peroxide both within and in the absence

Dr. A. Nourhani, D. Brown, N. Pletzer, Prof. J. G. Gibbs
Department of Physics and Astronomy
Northern Arizona University
Flagstaff, AZ 86011, USA
E-mail: john.gibbs@nau.edu

The ORCID identification number(s) for the author(s) of this article can be found under https://doi.org/10.1002/adma.201703910.

DOI: 10.1002/adma.201703910

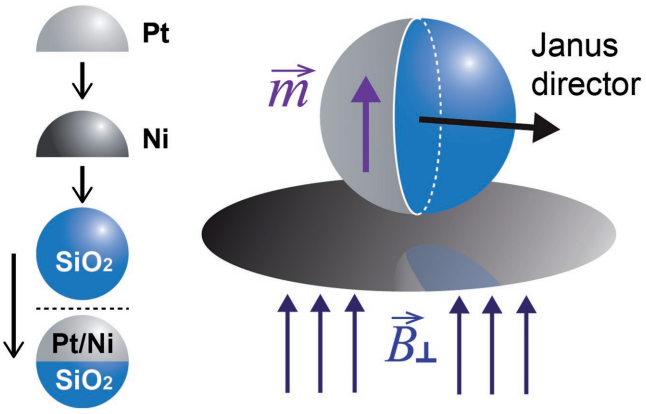

Figure 1. Left: the schematic shows the fabrication steps: 50 nm of Ni was deposited onto a monolayer of silica, SiO_2, microspheres. Then a 10 nm layer of Pt was deposited on top of the Ni. The final structure is a bi-metallic Janus sphere (bottom-left) with the Pt on the outer hemispherical surface. Right: when subjected to an external magnetic field perpendicular to the plane of motion, a particle's dipole moment, $\vec{m}$, aligns with the field. Due to the anisotropic coating, the dipole moment is shifted away from the center of the sphere. The Janus director, which defines the propulsion direction, points from the metal to the dielectric hemisphere.

of a magnetic field. For example, in 20% hydrogen peroxide, the particles moved with an average speed of ≈7 μm s^{-1}.

We applied a magnetic field, $\vec{B}_\perp$, to the unmagnetized particles that was perpendicular to the surface over which they moved. We used a vertically oriented Helmholtz coil pair in order to supply a uniform magnetic field; therefore, the field merely served to induce dipole moments in the particles as well as to align them with the field. As shown on the right side of Figure 1, the magnetic dipole $\vec{m}$ aligns vertically parallel to $\vec{B}_\perp$ and perpendicular to the Janus director, thus it cannot affect the direction of powered motion of an isolated active Janus sphere in the horizontal plane. Thus, the 2D deterministic motion was observed to be independent of $\vec{B}_\perp$. More specifically, a particle still swam away from the metal cap in a horizontal plane containing the Janus director, and was free to rotate about any vertical axis parallel to $\vec{B}_\perp$, identical to the behavior of the unmagnetized particles. It should be noted that the use of a magnetic field in systems of artificial active colloids is not new per se, as external fields have been used to guide nanomotors with a ferromagnetic component in unbounded domains[44] and through microchannels.[21] However, in these studies, the magnetic field was applied in the plane of motion in order to steer the particles and dictate their direction of propulsion. The critical distinction between such studies and ours stems from the direction of the applied magnetic field and its effect on particle–particle interactions.

The vertically aligned field in our system instead induces strong magnetic dipole–dipole interactions between neighboring particles resulting in a repulsive force that prevents direct contact. As the particles are not magnetized before the application of $\vec{B}_\perp$, and because they are situated in a plane perpendicular to the applied field, once the dipoles are induced by $\vec{B}_\perp$, the dipole–dipole interactions are repulsive only. Moreover, and critical to this study, the dipole moment in a Janus sphere morphology is also displaced from the center of the sphere.[45] As such, the same dipole–dipole repulsion that prevents the particles from self-assembling also applies a torque that alters the direction of motion. In our system, this torque aligns the particles' Janus directors toward other particles, leading to an effective "attraction." These combined effects lead to unique particle–particle interactions such as head-to-head reorientation, chasing, and contactless aggregation.

Thus, contrary to single particle motion, the dynamics of interacting particles was drastically altered by the external field. We observed three main phenomena arising from the magnetic dipole–dipole interactions between the particles: (1) dipole–dipole torque aligns the dielectric side (head) of two Janus spheres head-to-head, (2) effective long-range "attraction" results from coupling between powered motion and head-to-head alignment, and (3) the dipole–dipole repulsion, in most cases, prohibits contact between particles. Particles propelled by the chemical reaction in the absence of $\vec{B}_\perp$ did not exhibit any of these effects.

As shown in **Figure 2**a, as two isolated particles approach each other by chemically powered motion the magnetic dipole–dipole interaction grows stronger causing the pair to briefly become locked in a stable mutual orbit. The pair slightly turns clockwise with the two particles touching only briefly. The dipole–dipole repulsion quickly pushes them apart and the temporarily stabilized pair spins counterclockwise before thermal fluctuation of the direction of motion overcomes the magnetic torque and the two particles part ways. Most of the observed pairs maintained a stably locked head-to-head conformation, as demonstrated in the frames of Figure 2c. The repulsive dipole–dipole interaction also results in an applied torque about the center of each Janus sphere, thus ultimately orienting the particles head-to-head. Note that all of the video frames in this study have been enhanced from the originals in order to clearly distinguish the particles and orientations. A discussion of this process, figures with the original frames, as well as the original videos can be found in the Supporting Information.

When we encounter an equilibrium distance between two particles, intuitively we expect the presence of at least a repulsive and an attractive force. Electrostatic interactions are screened in solution and their range is smaller than the dipole–dipole short-range repulsion, so in the length scale of the interparticle distance, they are relatively negligible. Thus, we only have magnetic dipole–dipole repulsion and a counteracting attractive term that is not a real attractive force but a combination of the Janus spheres' motive force and the antiparallel alignment of the particles' Janus directors. We call this combination a pseudoforce that brings the particles together from long distances and becomes more effective in locking the particles into head-to-head pairs as two particles approach one another.

The motive force increases with fuel concentration $C_{H_2O_2}$ as $F_{motive} \propto C_{H_2O_2}/(1+\beta C_{H_2O_2})$ where β is a constant.[46] The repulsive magnetic force scales as $F_{mag} \propto R^{-4}$ where R is the distance between the dipoles and r is the distance from the center of the sphere to its net dipole position (see Figure 2g). As the pseudoforce is a function of the magnitude of the propulsion, with an increase in hydrogen peroxide concentration, we expect to see a decrease in the interparticle distance, as we

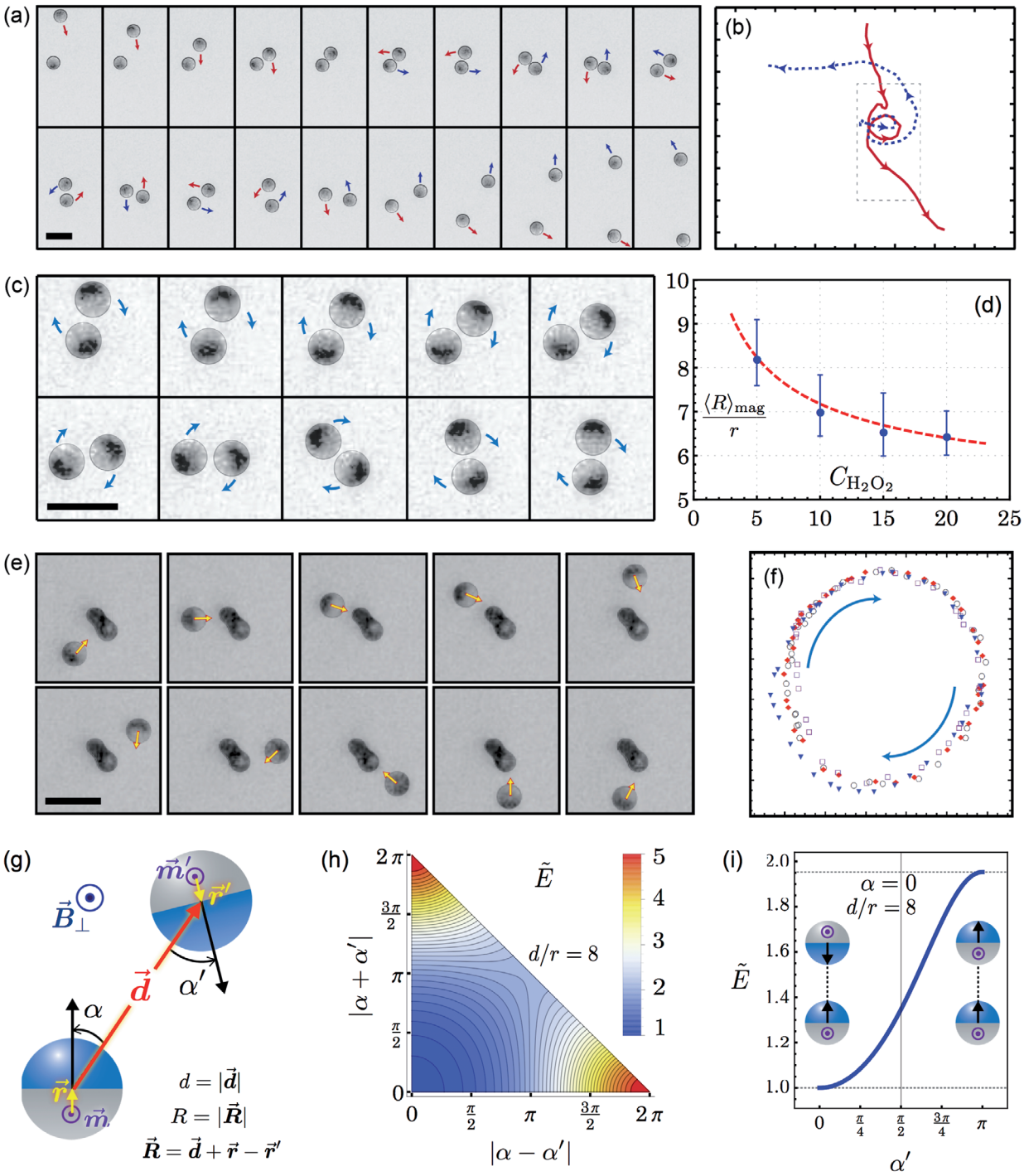

Figure 2. Interactions between two particles, or pair-interactions: a) Video frames showing two particles approaching one another, spinning about a mutual axis, then escaping. b) The plot shows the trajectories of the two particles in (a). The rectangular box shows the area of the trajectories represented in the frames. c) Video frames showing two particles spinning about a mutual axis while maintaining a fixed distance via dipole–dipole repulsion. Note the relative orientations remain approximately fixed. d) Concentration dependence of the spacing between particles in a pair showing that as activity increases, the separation decreases. The dashed red line is a fit of Equation (1) to the data. e) "Tidally locked" orbiting of a single particle around an immobilized cluster of magnetized particles. The Janus director, shown as a yellow arrow with a red outline, remains roughly locked toward the particle cluster. f) A 2D plot tracking the location of the orbiting particle in (e) with each shape/color representing a single rotation of four total rotations. The arrows indicate the clockwise orbital motion. g) Definition of the relative angles between two particles and the center-to-center vector, $\vec{d}$. The schematic also shows the offset, $\vec{r}$, of the dipole moments from the center of the spheres. h) Density plot of the dimensionless interaction energy. i) Dimensionless interaction energy with insets showing two example configurations, head-to-head and head-to-tail on the left and right side, respectively. Scale bar in (a), (c), and (e) = 5 μm.

observed in Figure 2d. Equating the counteracting motive and magnetic forces averaged over pairs at each fuel concentration, and fitting the resulting expression to the experimental data, yields

$$\frac{\langle R\rangle_{\mathrm{mag}}}{r}\propto\left(\frac{1+0.0365\,C_{\mathrm{H_2O_2}}}{C_{\mathrm{H_2O_2}}}\right)^{1/4} \tag{1}$$

which is plotted as the red dashed curve in Figure 2d and demonstrates the trend very well. $\langle R\rangle_{\mathrm{mag}}$ is the average dipole-to-dipole distance based on the average dipole force $\langle F_{\mathrm{mag}}\rangle$ of pairs such that $\langle F_{\mathrm{mag}}\rangle\propto\langle R\rangle_{\mathrm{mag}}^{-4}$ (see Supporting Information for the derivation of $\langle R\rangle_{\mathrm{mag}}$ and the calculation of the data in Figure 2d). To calculate r, we made the approximation that the net magnetic moment is located at the center of mass of the ferromagnetic layer,[47] giving a value of $r\simeq 0.8$ μm.

A locked pair of idealized Janus spheres, with perfect symmetry, would approach one another and remain stationary at a fixed equilibrium distance. We observed many such pairs. However, in the examples shown in the video frames of Figure 2a,c, the rotational motion is likely provided by slight asymmetries in the fabrication process leading to a propulsive torque applied to the Janus spheres. This suggests a design scheme for engineering modes of motion by intentionally introducing asymmetries in active particles.

To further illustrate alignment, locking, and the effect of slight asymmetry, the frames in Figure 2e show a single particle moving in a stable orbital pattern around a cluster of particles, which is immobilized on the surface and also has a vertical magnetic moment. The orbiting active particle shows an analogous "tidal locking" in that the same face is oriented approximately toward the cluster at all points of its trajectory. The arrows overlaying the frames show that the orientation of the Janus director remains radially inward toward the cluster, but the overall motion is roughly circular, as shown in Figure 2f. This orbital motion is a result of the Janus director not pointing exactly at the cluster at all times, as can be seen in Figure 2e. The plot in Figure 2f shows a total of four periods, with each full period indicated by a different symbol and color, giving a sense of the regularity of the orbital motion.

Now, let's quantitatively discuss the underlying mechanism for our observations. As shown in the schematic of Figure 2g, we denote the center-to-center vector from the unprimed (bottom) to the primed sphere (top) as $\vec{d}$ and the vectors connecting the dipole position to the center of the corresponding spheres as $\vec{r}$ and $\vec{r}'$. The separation vector of the dipoles, $\overline{m}$ and $\overline{m}'$, is given by $\vec{R}=\vec{d}+\vec{r}-\vec{r}'$. For simplicity, we assume the particles are identical and so $r=|\vec{r}|=|\vec{r}'|$.

Since magnetic interactions are not screened in solution,[48,49] the magnitude of the magnetic dipole–dipole force is $F_{\mathrm{mag}}=3\mu_0\overline{m}^2/(4\pi R^4)$ where $\overline{m}=\sqrt{\vec{m}\cdot\vec{m}'}=\sqrt{mm'}$ is the geometric average of the magnetic moments and μ_0 is the magnetic constant. At low Reynolds number flow, the magnitude of the motive, F_{mot}, and drag forces are equal for a particle of radius a and moving at speed v in a fluid of viscosity η; thus, $F_{\mathrm{mot}}=6\pi\eta av$. By equating the motive and dipole–dipole repulsion forces at equilibrium, we can approximate the average magnetic moment as

$$\overline{m}\simeq\langle R\rangle_{\mathrm{mag}}^2\left(\frac{8\pi\eta av}{\mu_0}\right)^{1/2} \tag{2}$$

Using the parameter values $\eta=8.90\times10^{-4}$ Pa s, $\mu_0=4\pi\times10^{-7}$ m kg s^{-2}A^{-2}, along with the experimental data $a=1.1$ μm, $v=7$ μm s^{-1}, and $\langle R\rangle_{\mathrm{mag}}\simeq 5.17$ μm at fuel concentration $C_{\mathrm{H_2O_2}}=20\%$ and an applied magnetic field $B_\perp\simeq10^{-2}$ T, we obtain $\overline{m}\simeq 9.8\times10^{-15}$ N m T^{-1}. The dipole moment at saturation for a Janus sphere with Ni of highest thickness $t=50$ nm is $m_{\mathrm{s}}=\gamma\frac{2\pi}{3}a^2tM_{\mathrm{s}}=6.2\gamma\times10^{-14}$ N m T^{-1}, where $M_{\mathrm{s}}=4.9\times10^5$ A m^{-1} for the magnetic saturation of Ni[50] and $\gamma<1$ is a shape factor resulting from averaging over the direction of magnetic dipoles inside the Ni shell. In this calculation, we have used the volume of half a spheroidal shell, as explained in the Supporting Information.

At a field strength of ≈10 mT, we expect to be close to saturation of Ni for Janus particles.[45] Along the axis perpendicular to the Janus director, the coercivity of the Ni cap is low as this is the "easy axis" of such a morphology. Our measured average magnetic dipole is off by an order-one factor $m_{\mathrm{s}}/\overline{m}=6.26\gamma$. We may attribute the discrepancy to a few causes such as partial magnetic saturation of the Ni layer, error in measurement, geometrical effects, approximations, and possible contributions from colloidal and hydrodynamic forces. The proportions of these effects on the discrepancy are not presently clear.

To further understand our observations, the next step is to study the conformation energy

$$E=10^{-3}\frac{\mu_0\overline{m}^2}{4\pi r^3}\tilde{E}\left(\frac{d}{r},\alpha,\alpha'\right) \tag{3}$$

of the dipoles. The energy scale $10^{-3}\mu_0\overline{m}^2/(4\pi r^3)$ is about 0.1 eV. The order-one function $\tilde{E}=10^3/\tilde{R}^3$ is the dimensionless conformation energy, plotted in Figure 2h, and the dimensionless dipole-to-dipole distance is defined by

$$\tilde{R}=\left\{\frac{d^2}{r^2}+4\cos^2\left[\frac{\alpha-\alpha'}{2}\right]+4\frac{d}{r}\cos\left[\frac{\alpha-\alpha'}{2}\right]\cos\left[\frac{\alpha+\alpha'}{2}\right]\right\}^{1/2} \tag{4}$$

See Supporting Information for the derivation of Equation (4). Similar to our recent study on Janus sphere dimer conformations, the parameter subspace (α, α') of $\tilde{E}$ can be reduced by symmetry arguments.[37] $\tilde{E}$ depends on the absolute difference $|\alpha-\alpha'|$ and sum $|\alpha+\alpha'|$ of the conformation angles α and α', as is explicit in Equation (4).

The conformation energy can explain the stability of the head-to-head conformations. All the pairs we observed were in this conformation for which dipole–dipole torque is zero. Even though the head-to-tail conformation also has zero torque, we never observed this in our experiments. Figure 2i shows the dimensionless magnetic interaction energy of two Janus spheres with fixed $d/r=8$. The Janus director of the unprimed sphere is aligned with the center-to-center vector ($\alpha=0$) and the Janus director of the primed sphere varies such that the pair conformation changes from head-to-head ($\alpha'=0$) to head-to-tail ($\alpha'=\pi$). Any deviation from the head-to-head conformation

results in an increase in the conformation energy, and even though the head-to-tail conformation has zero dipole–dipole torque, it has the highest conformation energy and is therefore very unstable. What can be gleaned from this analysis is that pairs of particles should align antiparallel, which is what we have observed, as this configuration minimizes the energy of the system.

We now show that our system can be exploited for useful applications. For example, the majority of studies on microscale cargo delivery have been based upon attaching a cargo to an active swimmer.[20–24,51,52] Here, on the other hand, we can transport passive cargo that has a magnetic dipole. An active Janus sphere can "push" such cargo remotely without any contact. Since the dipole–dipole torque aligns the Janus director toward the cargo, mild thermal noise does not lead to the dissociation of the pair.

To demonstrate the feasibility of this application, we made a mixed population of our active Janus and passive spherical magnetic particles in a hydrogen peroxide solution. An example of the result is shown in **Figure 3**a, in which an active particle "pushes" a passive cargo. The passive magnetic particles were observed to move with Brownian motion only until an active Janus particle approached. Subsequently, the dipole repulsion between the particles resulted in the passive one being continuously pushed away from the active particle. Over the frames, we have placed adjacent shadow images of the two particles to show the behavior in clearer detail. We have indicated the Janus director as a yellow arrow with a red outline and the cargo as a dashed blue circle. To the best of our knowledge, this is the first example of contactless cargo delivery at the microscale.

Another unique phenomena of our system is "chasing." That is, active swimmers were observed pursuing mobile magnetic particles, as demonstrated in the video frames of Figure 3b. A cluster of two self-assembled particles is swimming roughly linearly (upward in the frames), and a single active particle is homing-in and chasing the cluster. Similar to the pushing phenomenon, the active particle chases the cluster by maintaining its Janus director toward the assembly regardless of any changes in velocity the cluster makes. We note that the hydrodynamic flow field at the rear of the cluster is expected to be repelling,[53,54] and therefore the chasing particle must overcome this field in order for the chasing effect to be possible. It should also be noted this cluster consists of two particles that are in contact with one another, in which the self-assembly likely occurred before the field was applied.

As we increased the density of particles, we observed more complex multiparticle interactions. When several particles interacted, they did not self-assemble into close-packed clusters, as was observed when $\vec{B}_{\perp}$ was absent. However, the particles collapsed into such closely packed clusters when the field was removed, or was reoriented parallel to the plane of motion. The clusters became partially disassembled with the reapplication of the perpendicular field, showing the effect is, in part, reversible. However, many remained self-assembled due to the particles retaining dipole moments after field removal. We show examples of multiparticle behavior in Figure 3.

In Figure 3c, we show the approach of a single particle to a stable pair, which then forms a three-particle assembly that remains stable and mostly stationary. On the far right side of Figure 3c, we show a schematic of an idealized stable three-particle assembly in which the Janus directors do not point antiparallel, as in the case of pair-interactions, but instead point toward a common center. This is expected to be the lowest energy configuration for three particles. When slight asymmetries and noise are combined, three-particle assemblies often showed more dynamic behavior, as seen in Figure 3d. In comparison to the particles in Figure 3c, this cluster actively changes its configuration over time. The arrows in the figure show the instantaneous velocities for each particle.

Finally in Figure 3e, we show a cluster of seven particles that have multibody interactions demonstrating much more dynamic behavior. The dynamic cluster continuously morphs into various shapes as a result of the balance between the attractive and repulsive forces between all of the particles in the group. In Figure 3e, we have overlaid two particles with dashed, colored lines in order to help distinguish the dynamic motion. We emphasize that the contactless interaction between the particles is critical for the dynamics of such a cluster as the particles are able to easily move past others without becoming jammed.

In conclusion, we have designed a system of active colloidal swimmers that interact and self-assemble without coming into direct contact. This was achieved by applying a magnetic field perpendicular to the plane of motion of self-phoretic, magnetic and catalytic Janus particles. We engineered this system so that the particles respond strongly to neighboring particles via magnetic dipole–dipole interaction, while previous studies in the field primarily relied upon center-to-center monopole interactions to investigate collective behavior of active colloids. Furthermore, since the dipole moment is a function of both the thickness and the magnetic properties of the material, the dipole–dipole interactions can be further engineered by altering these parameters. The interplay of the effective attraction-induced pseudoforce and a magnetic repulsive force, as well as the collective motion of the particles, introduces unique modes of motion that provides a new paradigm for this field. Our future plans include quantifying the collective behavior of large numbers of such particles as well as engineering new modes of motion.

Experimental Section

To fabricate the Janus particles, first a monolayer of silica microspheres of average diameter 2.2 μm was deposited onto a Si(100) silicon wafer by a Langmuir–Blodgett method. Next, 50 nm of Ni and 10 nm of Pt were deposited by electron beam evaporation at a pressure of ≈10^{-5} Torr. The Pt was deposited after the Ni so the Pt forms on the outer surface. The particles were left unmagnetized at this point to prevent aggregation when suspended in water. A small segment of the wafer of dimension ≈1cm × 1cm and ≈1mL of 18 MΩ water were combined in a glass vial. Colloidal suspensions of the Janus spheres were obtained by placing the vial into a bath sonicator for ≈1 min to remove a substantial fraction of the particles from the solid surface into the water.

The particles were observed moving on either a glass microscope slide or the polished face of a Si(100) silicon wafer. The glass slides were washed with water and soap followed by ethanol and drying with nitrogen gas. Both the glass slides and silicon wafers were cleaned

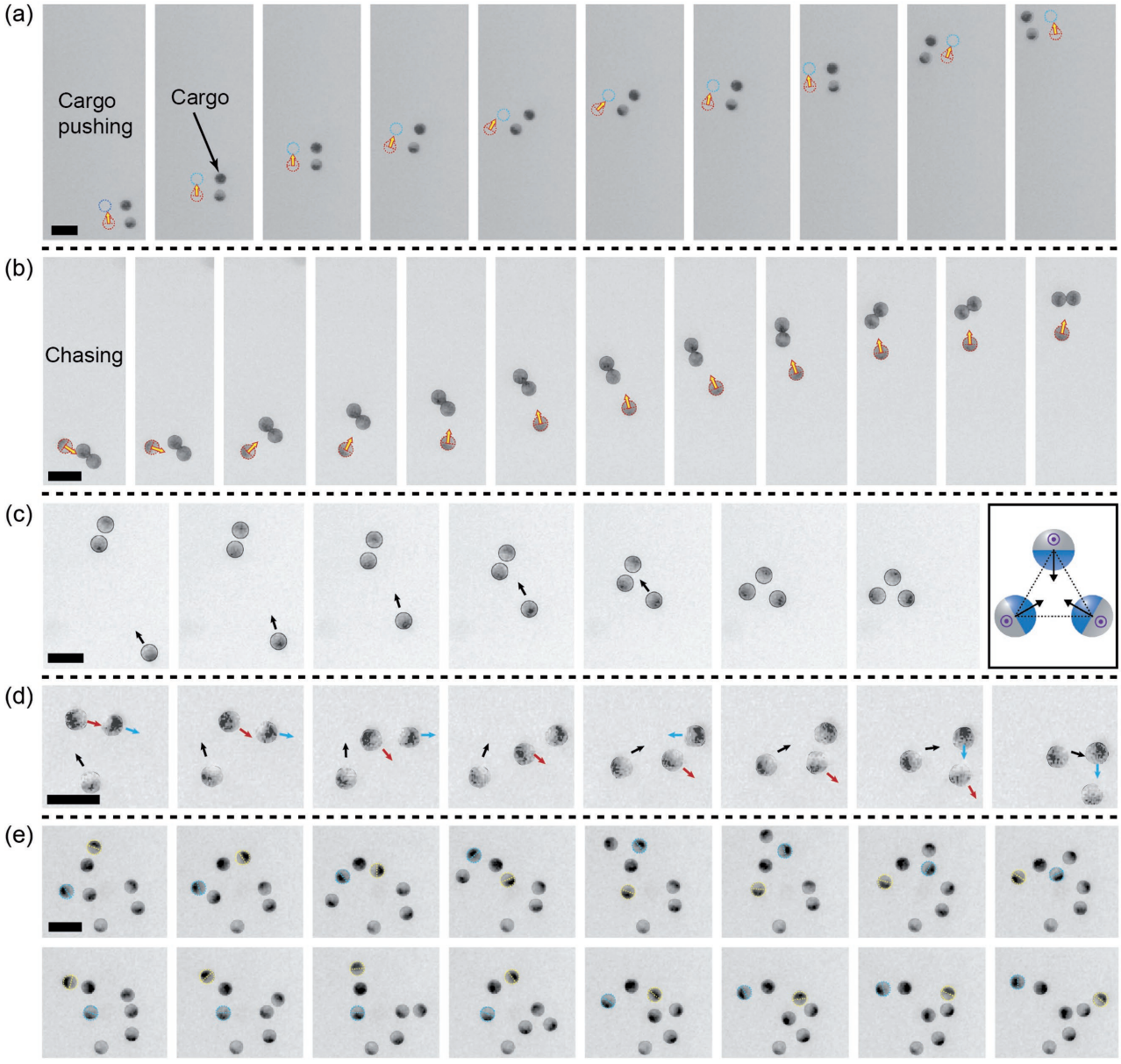

Figure 3. Example enhanced video frames showing interactions of multiple particles. a) A single active particle "pushes" a passive spherical magnetic particle, as a demonstration of contactless cargo delivery. Shadow particles are shown next to the actual ones: dashed blue indicates the cargo, and the pushing particle is dashed red and has a yellow vector with a red outline indicating the Janus director. b) A pair of particles moves independently from the bottom of the frames to the top as time progresses. A single active particle "chases" this pair by constantly reorienting its direction of motion toward the pair. The Janus director is drawn as a yellow vector with a red outline. c) A pair of particles has a roughly fixed orientation. A third particle approaches the pair with velocity direction indicated by the black arrows. The single particle and the pair form a triplet configuration. The schematic on the right shows an idealized triplet. d) An example triplet configuration in which fluctuations in the propulsion directions of the particles lead to the cluster rearranging in space as time progresses. The arrows indicate the velocity directions at each particular frame. e) More complex patterns emerge from the interaction of many particles. Two particles, chosen at random, have been color-coded to aid the eye in distinguishing the dynamics of the cluster. Scale bars = 5 μm.

with oxygen plasma before pipetting the colloidal suspension onto the solid surfaces. Various concentrations of hydrogen peroxide were prepared by diluting stock 30% (v/v) H_2O_2 with pure water, and were mixed with the colloids. A Helmholtz coil pair was aligned vertically to generate a magnetic field antiparallel to gravity. An upright microscope was placed entirely within the coil pair to ensure field-uniformity at the location of the sample. The current in the coil fell in the range of 0–10 A which produced DC magnetic fields of 0–10 mT. The motion of the particles was recorded with a camera at a frame rate of 15 fps, and a 50 × long-working-distance objective was employed. We processed the videos using the free software ImageJ.

Supporting Information

Supporting Information is available from the Wiley Online Library or from the author.

Acknowledgements

This study was based upon the work supported in part by the National Science Foundation under Grant No. CBET-1703322 and in part by the State of Arizona Technology and Research Initiative Fund (TRIF), administered by the Arizona Board of Regents (ABOR). The authors would also like to give a special thanks to Dr. Paul E. Lammert for his insightful discussions and suggestions.

Conflict of Interest

The authors declare no conflict of interest.

Keywords

active matter, contactless interactions, dipole alignment, magnetic Janus particles

Received: July 13, 2017
Revised: September 11, 2017
Published online:

[1] T. R. Kline, W. F. Paxton, T. E. Mallouk, A. Sen, *Angew. Chem., Int. Ed.* **2005**, *44*, 744.
[2] Y. He, J. Wu, Y. Zhao, *Nano Lett.* **2007**, *7*, 1369.
[3] A. A. Solovev, S. Sanchez, M. Pumera, Y. F. Mei, O. G. Schmidt, *Adv. Funct. Mater.* **2010**, *20*, 2430.
[4] D. P. Singh, U. Choudhury, P. Fischer, A. G. Mark, *Adv. Mater.* **2017**, *20*, 1701328.
[5] T.-C. Lee, M. Alarcón-Correa, C. Miksch, K. Hahn, J. G. Gibbs, P. Fischer, *Nano Lett.* **2014**, *14*, 2407.
[6] S. Sanchez, L. Soler, J. Katuri, *Angew. Chem., Int. Ed.* **2015**, *54*, 1414.
[7] M. Alarcón-Correa, D. Walker, T. Qiu, P. Fischer, *Eur. Phys. J.: Spec. Top.* **2016**, *225*, 2241.
[8] X. Lin, Z. Wu, Y. Wu, M. Xuan, Q. He, *Adv. Mater.* **2016**, *28*, 1060.
[9] S. Sanchez, A. A. Solovev, S. M. Harazim, O. G. Schmidt, *J. Am. Chem. Soc.* **2010**, *133*, 701.
[10] S. Sanchez, A. A. Solovev, S. Schulze, O. G. Schmidt, *Chem. Commun.* **2011**, *47*, 698.
[11] J. Gibbs, P. Fischer, *Chem. Commun.* **2015**, *51*, 4192.
[12] U. Choudhury, L. Soler, J. G. Gibbs, S. Sanchez, P. Fischer, *Chem. Commun.* **2015**, *51*, 8660.
[13] D. Walker, M. Kubler, K. Morozov, P. Fischer, A. Leshansky, *Nano Lett.* **2015**, *15*, 4412.
[14] D. Vilela, J. Parmar, Y. Zeng, Y. Zhao, S. Sánchez, *Nano Lett.* **2016**, *16*, 2860.
[15] J. Wang, *ACS Nano* **2009**, *3*, 4.
[16] S. Tottori, L. Zhang, F. Qiu, K. K. Krawczyk, A. Franco-Obregón, B. J. Nelson, *Adv. Mater.* **2012**, *24*, 811.
[17] L. Berthier, J. Kurchan, *Nat. Phys.* **2013**, *9*, 310.
[18] B. Jurado-Sánchez, S. Sattayasamitsathit, W. Gao, L. Santos, Y. Fedorak, V. V. Singh, J. Orozco, M. Galarnyk, J. Wang, *Small* **2015**, *11*, 499.
[19] F. Qiu, S. Fujita, R. Mhanna, L. Zhang, B. R. Simona, B. J. Nelson, *Adv. Funct. Mater.* **2015**, *25*, 1666.
[20] S. Sundararajan, P. E. Lammert, A. W. Zudans, V. H. Crespi, A. Sen, *Nano Lett.* **2008**, *8*, 1271.
[21] J. Burdick, R. Laocharoensuk, P. M. Wheat, J. D. Posner, J. Wang, *J. Am. Chem. Soc.* **2008**, *130*, 8164.
[22] L. Zhang, T. Petit, Y. Lu, B. E. Kratochvil, K. E. Peyer, R. Pei, J. Lou, B. J. Nelson, *ACS Nano* **2010**, *4*, 6228.
[23] S. Sundararajan, S. Sengupta, M. E. Ibele, A. Sen, *Small* **2010**, *6*, 1479.
[24] X. Ma, K. Hahn, S. Sanchez, *J. Am. Chem. Soc.* **2015**, *137*, 4976.
[25] D. Kagan, P. Calvo-Marzal, S. Balasubramanian, S. Sattayasamitsathit, K. M. Manesh, G.-U. Flechsig, J. Wang, *J. Am. Chem. Soc.* **2009**, *131*, 12082.
[26] J. Wu, S. Balasubramanian, D. Kagan, K. M. Manesh, S. Campuzano, J. Wang, *Nat. Commun.* **2010**, *136*.
[27] H.-H. Jeong, A. G. Mark, T.-C. Lee, M. Alarcón-Correa, S. Eslami, T. Qiu, J. G. Gibbs, P. Fischer, *Nano Lett.* **2016**, *16*, 4887.
[28] D. Schamel, A. G. Mark, J. G. Gibbs, C. Miksch, K. I. Morozov, A. M. Leshansky, P. Fischer, *ACS Nano* **2014**, *8*, 8794.
[29] Y. Hong, M. Diaz, U. M. Córdova-Figueroa, A. Sen, *Adv. Funct. Mater.* **2010**, *20*, 1568.
[30] W. Wang, W. Duan, A. Sen, T. E. Mallouk, *Proc. Natl. Acad. Sci.* **2013**, *110*, 17744.
[31] S. Thakur, R. Kapral, *Phys. Rev. E* **2012**, *85*, 026121.
[32] A. A. Solovev, S. Sanchez, O. G. Schmidt, *Nanoscale* **2013**, *5*, 1284.
[33] W. Wang, W. Duan, S. Ahmed, A. Sen, T. E. Mallouk, *Acc. Chem. Res.* **2015**, *48*, 1938.
[34] J. Palacci, S. Sacanna, A. P. Steinberg, D. J. Pine, P. M. Chaikin, *Science* **2013**, *339*, 936.
[35] I. Buttinoni, J. Bialké, F. Kümmel, H. Löwen, C. Bechinger, T. Speck, *Phys. Rev. Lett.* **2013**, *110*, 238301.
[36] J. Elgeti, R. G. Winkler, G. Gompper, *Rep. Prog. Phys.* **2015**, *78*, 056601.
[37] J. N. Johnson, A. Nourhani, R. Peralta, C. McDonald, B. Thiesing, C. J. Mann, P. E. Lammert, J. G. Gibbs, *Phys. Rev. E* **2017**, *95*, 042609.
[38] Y. Wu, Z. Wu, X. Lin, Q. He, J. Li, *ACS Nano* **2012**, *6*, 10910.
[39] L. Baraban, R. Streubel, D. Makarov, L. Han, D. Karnaushenko, O. G. Schmidt, G. Cuniberti, *ACS Nano* **2013**, *7*, 1360.
[40] H. Ke, S. Ye, R. L. Carroll, K. Showalter, *J. Phys. Chem. A* **2010**, *114*, 5462.
[41] A. Nourhani, P. E. Lammert, *Phys. Rev. Lett.* **2016**, *116*, 178302.
[42] S. Das, A. Garg, A. I. Campbell, J. Howse, A. Sen, D. Velegol, R. Golestanian, S. J. Ebbens, *Nat. Commun.* **2016**, *6*, 8999.
[43] J. Simmchen, J. Katuri, W. E. Uspal, M. N. Popescu, M. Tasinkevych, S. Sánchez, *Nat. Commun.* **2016**, *7*, 10598.
[44] P. Dhar, T. M. Fischer, Y. Wang, T. Mallouk, W. Paxton, A. Sen, *Nano Lett.* **2006**, *6*, 66.
[45] J. Yan, S. C. Bae, S. Granick, *Adv. Mater.* **2015**, *27*, 874.
[46] A. Nourhani, V. H. Crespi, P. E. Lammert, *Phys. Rev. E* **2015**, *91*062303.
[47] A. I. Campbell, S. J. Ebbens, *Langmuir* **2013**, *29*, 14066.
[48] S. K. Smoukov, S. Gangwal, M. Marquez, O. D. Velev, *Soft Matter* **2009**, *5*, 1285.
[49] S. Sacanna, L. Rossi, D. J. Pine, *J. Am. Chem. Soc.* **2012**, *134*, 6112.
[50] H. Kronmuller, M. Fahnle, *Micromagnetism and the Microstructure of Ferromagnetic Solids*, Cambridge Studies in Magnetism, Cambridge University Press, Cambridge **2003**.
[51] L. Baraban, D. Makarov, R. Streubel, I. Monch, D. Grimm, S. Sanchez, O. G. Schmidt, *ACS Nano* **2012**, *6*, 3383.
[52] T. Yang, T. O. Tasci, K. B. Neeves, N. Wu, D. W. Marr, *Langmuir* **2017**, *33*, 5932.
[53] A. Nourhani, P. E. Lammert, V. H. Crespi, A. Borhan, *Phys. Fluids* **2015**, *27*, 012001.
[54] A. Nourhani, V. H. Crespi, P. E. Lammert, A. Borhan, *Phys. Fluids* **2015**, *27*, 092002.

